AIP | Journal of Applied Physics

Effect of Si-doping on InAs nanowire transport and morphology

S. Wirths, K. Weis, A. Winden, K. Sladek, C. Volk et al.

Citation: J. Appl. Phys. **110**, 053709 (2011); doi: 10.1063/1.3631026
View online: http://dx.doi.org/10.1063/1.3631026
View Table of Contents: http://jap.aip.org/resource/1/JAPIAU/v110/i5
Published by the American Institute of Physics.

Effect of Si-doping on InAs nanowire transport and morphology

S. Wirths,[1] K. Weis,[1] A. Winden,[1] K. Sladek,[1] C. Volk,[1] S. Alagha,[1] T. E. Weirich,[2] M. von der Ahe,[1] H. Hardtdegen,[1] H. Lüth,[1] N. Demarina,[1] D. Grützmacher,[1] and Th. Schäpers[1,a)]

[1]*Peter Grünberg Institute (PGI-9), Forschungszentrum Jülich, 52425 Jülich, Germany and JARA-Fundamentals of Future Information Technology, Jülich-Aachen Research Alliance, Germany*
[2]*Central Facility for Electron Microscopy and Institute of Crystallography, RWTH Aachen University, Germany and JARA-Fundamentals of Future Information Technology, Jülich-Aachen Research Alliance, Germany*

(Received 24 June 2011; accepted 26 July 2011; published online 12 September 2011)

The effect of Si-doping on the morphology, structure, and transport properties of nanowires was investigated. The nanowires were deposited by selective-area metal organic vapor phase epitaxy in an N_2 ambient. It is observed that doping systematically affects the nanowire morphology but not the structure of the nanowires. However, the transport properties of the wires are greatly affected. Room-temperature four-terminal measurements show that with an increasing dopant supply the conductivity monotonously increases. For the highest doping level the conductivity is higher by a factor of 25 compared to only intrinsically doped reference nanowires. By means of back-gate field-effect transistor measurements it was confirmed that the doping results in an increased carrier concentration. Temperature dependent resistance measurements reveal, for lower doping concentrations, a thermally activated semiconductor-type increase of the conductivity. In contrast, the nanowires with the highest doping concentration show a metal-type decrease of the resistivity with decreasing temperature. © *2011 American Institute of Physics*. [doi:10.1063/1.3631026]

I. INTRODUCTION

Without any doubt, semiconductor nanowires can be regarded as very promising candidates for the realization of future high-performance nanoelectronic devices.[1] This is because the bottom-up approach employed for their growth has the potential to simplify the device processing scheme substantially and, more importantly, material combinations are allowed that find no counterpart in epitaxial semiconductor layer systems.[2–4] In fact, in recent years field-effect transistors based on semiconductor nanowires have already been demonstrated.[5–10] Apart from these more conventional applications semiconductor nanowires are also very promising to explore the possible realization of devices based on quantum effects.[11–18] The large surface-to-volume ratio of semiconductor nanowires implies that surface properties have a large impact on the transport properties. In this respect, low band-gap III-V semiconductors, e.g., InAs, InN, or InSb, are often the focus of interest because for 2- or 3-dimensional systems, the Fermi level at the surface is pinned inside the conduction band. As a consequence, an electron accumulation layer is formed at the surface.[19] It can therefore be expected that the conductance of the nanowire is sufficiently large even at low nanowire radii and that the nanowires are not depleted at room temperature.[2,20–22] However, in the past we have found out that our InAs nanowires deposited using selective-area metalorganic vapor phase epitaxy (SA-MOVPE) do not exhibit the expected quasi-metallic behavior. In contrast, they show semiconductor behavior, i.e., an increase of the resistance with decreasing temperature, and are quite resistive at room temperature.[23] The reason for the low conductivity of our nanowires is not clear, so far.

A number of possible reasons could be responsible for the result: first of all, the structure of the nanowires could explain their high resistivity. Many groups have demonstrated that InAs nanowires have the tendency to form stacking faults during growth, since the energetic difference between the zinc blende and the wurtzite phase is very small. Especially for thinner wires, a wurtzite structure is observed. Also, the growth conditions of the nanowires play a major role in their structural characteristics and the density of stacking faults.[24] Dayeh *et al.*[25] have stated that stacking faults and the accompanying rapid structural alternation from wurtzite to zinc blende should have a detrimental effect on conductivity. A further reason for the low conductivity could be the relatively low background doping level in our wires. The most common method for preparing InAs nanowires by MOVPE is the vapor-liquid-solid (VLS) growth method. Here, very low growth temperatures in the range of 400-450 °C are employed to produce the wires. It cannot be ruled out that the decomposition of the metalorganic sources is incomplete leading to an unintentional carbon (donor) incorporation and conductive InAs nanowires are observed by these groups. Tomioka *et al.*[26,27] and Peatzelt *et al.*[28] have employed SA-MOVPE to obtain InAs nanowires using H_2 as the ambient. Here, growth temperatures of 540-600 °C are used, which is higher than for VLS grown wires. However, these temperatures are still 50-110 °C lower than those we use in our study, taking advantage of modified gas phase reactions in an N_2 ambient.[29]

Typically, in this range of temperatures, the structural properties and background doping concentration improve for

a)Author to whom correspondence should be addressed. Electronic mail: th.schaepers@fz-juelich.de.

III/V semiconductors with increasing deposition temperatures. Thus, the lower conductivity found in our nanowires might be attributed to a lower background doping level. It is well known that the mobility of low-dimensional electron systems, i.e., 2-dimensional electron gases, decreases at very low carrier densities due to the localization of carriers in potential fluctuations of imperfect interfaces. In this respect it is desirable to control the carrier concentration in our wires. Thus, we investigated the influence of Si-doping on the nanowire electrical characteristics. This would supply us, on the one hand, with a first tool to design different types of nano- and opto-electronic devices. On the other hand,using a dopant may also help to provide answers to the question of why our nominally undoped nanowires are highly resistive. However, it has to be kept in mind that the doping of nanostructures may not only change the carrier concentration but also the morphology. Up to now, successful *n*- or *p*-type doping has already been reported for various III-V semiconductor nanowires, such as InAs,[7,30–32] GaAs,[33,34] or InN nanowires.[35] The doping of InAs nanowires by SA-MOVPE has not been reported, especially at the high growth temperature needed when using an N_2 ambient. Here, we studied the impact of Si doping on the nanowire morphology, structure, and conductivity. In order to minimize the large variance usually observed in the electrical data and to improve the reliability of the conclusions, a large number of nanowires were characterized electrically for each dopant concentration.

II. EXPERIMENTAL

The nanowires were grown on GaAs (111)B substrates by low-pressure MOVPE. Nitrogen (N_2) was used as the carrier gas to transport trimethylindium (TMIn) and arsine (AsH_3) into the reactor at a working pressure of 20 mbar and a total gas flow rate of 3100 ml/min. The precursor partial pressures were kept constant at 0.118 and 12.9 Pa, respectively, which results in a V/III ratio of 110. The growth temperature was 650 °C. The GaAs (111)B substrates were covered by a 30 nm thin patterned SiO_2 layer. The pattern consisted of hole arrays with about a 50 nm hole diameter and a 500 nm pitch, which was defined by electron beam lithography using positive resists and CHF_3 reactive ion etching. Prior to the growth, the samples were cleaned by H_2SO_4 and rinsed in de-ionized water; the details can be found in Ref. 29. For silicon doping during growth, the disilane (Si_2H_6) flux was adjusted to achieve various *n*-type doping levels. In order to quantify the supply of doping species more easily, we defined a doping factor, consisting of the partial pressure ratio of dopant versus group III precursor. A ratio of $p(Si_2H_6)/p(TMIn) = 7.5 \times 10^{-5}$ was set as the doping factor 1. Successively, the doping factor was varied from 0 to 500. For all growth runs a growth time of 3 min was maintained.

The morphology and structure of the nanowires have been investigated by scanning electron microscopy (SEM), transmission electron microscopy (TEM), and selected area electron diffraction (SAED). For the TEM investigation the nanowires were separated from the substrate and transferred to holey carbon film coated TEM grids. In all cases, we looked at the [1000] wurtzite and the [011] zinc blende zone axis, respectively, because in this direction stacking faults are clearly visible.[25]

For transport measurements, the nanowires were transferred onto an *n*-doped Si (100) wafer covered by a 100-nm-thick SiO_2 layer. The SiO_2 layer was prepared by thermal oxidation. The Si/SiO_2 substrate was patterned with contact pads and adjustment markers. The nanowires were contacted individually by a set of Ti/Au electrodes using electron beam lithography. If the wire length was sufficient, four contact fingers were placed on the nanowire to perform four-terminal transport measurements. Ar^+ sputtering was employed prior to the metal deposition, in order to remove residual impurities from the surface. For some measurements the substrate was used as a back-gate to control the electron concentration. In Fig. 1 an SEM image of a contacted nanowire is shown.

At room temperature two- and four-terminal measurements were performed, in order to determine the wire resistance using a dc probe station. For each set of nanowires with a particular doping factor, at least 20 nanowires were measured. By means of the four-terminal set-up the effect of the contact resistance can be eliminated. For low temperature measurements down to 4 K, a He-4 flow cryostat was employed.

III. MORPHOLOGY AND STRUCTURAL PROPERTIES

First, the effect of doping on the nanowire morphology and structure was investigated. The SEM images of the as-grown nanowires are shown in Fig. 2. In all cases we obtained hexagonally shaped wires, quite homogeneous in length and diameter, which stand vertically on the substrate. It is obvious that on the one hand, with an increasing doping factor the length of the nanowires decreases [cf., Figure 3 (lower inset)] whereas on the other hand, the diameter increases [cf., Figure 3 (upper inset)]. Thus, doping seems to affect the growth rates differently for different facet types, which leads to decreasing axial and increasing radial growth. Additionally, the average aspect ratio, L/d, between wire length, L, and diameter, d, does not change linearly with the doping concentration (see Fig. 3). The lowest doping factor of 1 leads to an aspect ratio of 54, which is reduced to 18 for a doping factor of 500. As a reference, for zero doping an aspect ratio of 100 was observed.[29] We also made a statistical evaluation of the nanowire dimensions. For each sample the length and diameter from 30 up to 40 wires were determined and the aspect ratio was calculated. The standard deviation

FIG. 1. (Color online) Scanning electron micrograph of an InAs nanowire with four contact fingers.

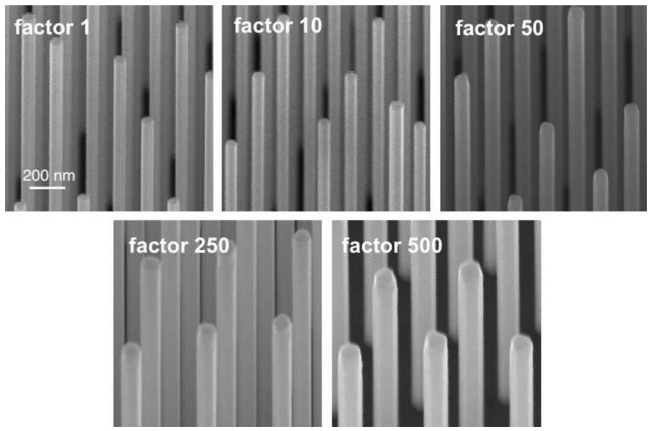

FIG. 2. Scanning electron micrographs of as-grown InAs nanowires for the doping factors of 1, 10, 50, 250, and 500.

of the aspect ratio decreases for the higher doping concentration as indicated by the bars in Fig. 3. Obviously, higher doping levels cause a more homogeneous nanowire growth, which could possibly be attributed to a lowered diffusion of group III material on the nanowire side facets and, therefore, to a reduced vertical growth rate. Further experiments need to be done to investigate this behavior. The TEM and SAED investigations clearly show that the growth direction for all nanowires is [111] and [0001] for the zinc blende and the wurtzite type, respectively.

The transmission electron micrographs (Fig. 4) show that for all doping factors the nanowires exhibit a large amount of stacking faults, which corresponds to a development of polytypism, or a change in the crystal structure from wurtzite to zinc blende segments and vice versa. The variance in structure exhibits no systematic dependence on the doping factor. Starting with undoped wires where a predominantly wurtzite structure is observed, the amount of zinc blende domains increases up to a doping factor of 100 while further doping again gives rise to more wurtzite type segments. For all nanowires we also performed SAED. The diffraction patterns of the [1000] wurtzite zone axis are presented below the TEM micrographs (see Fig. 4). A calculation of the lattice parameters of the InAs nanowires is possible from these patterns. The values for the c-lattice parameters are in good agreement with the theoretical value for calculated bulk wurtzite InAs, whereas the a-lattice parameter is shortened around 11%.[36]

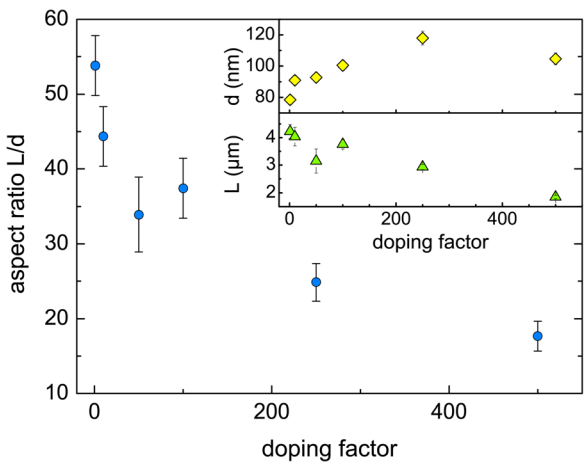

FIG. 3. (Color online) Average aspect ratio of nanowires plotted against the doping factor. Vertical bars represent standard deviations of the average values. The upper and lower insets show the average diameters and lengths vs doping factor, respectively.

IV. TRANSPORT PROPERTIES

In order to investigate the effect of Si-doping, we performed systematic transport measurements on a series of contacted nanowires with different doping factors. First, we will focus on the room temperature transport properties, while later on, the temperature dependence of the wire resistance is discussed in detail.

A. Room temperature transport

In order to exclude the contribution of the contact resistance, four-terminal measurements were performed to determine the resistivity, ρ_{3d}. Here, the outer contacts were used to feed a current through the nanowire, while the voltage drop was measured between the two inner contacts. In contrast to single-mode ballistic quantum wires,[37] the transport in our nanowires is diffusive with a large number of quantum channels so that in our case the four-terminal measurement configuration can be applied. In Fig. 5 the four-terminal resistance, R, of nanowires with a doping factor of 1, 50, 100, and 250 is plotted as a function of l/A, with l as the distance between the two voltage probe contacts and A as the area of the nanowire cross section. The resistance values obtained for undoped nanowires, i.e., a doping factor of 0, are not shown for clarity, since they are comparable with the ones determined for the set of samples with a doping factor of 1. On wires with a doping factor of 500, no four-terminal measurements could be performed owing to their insufficient length. As can be inferred from Fig. 5, for each set of wires with a particular doping factor, the resistance increases linearly on average with increasing l/A (see lines), which indicates a uniform conductance along the wire. The fact that Si was successfully incorporated as a dopant can be deduced from the observation that with increasing doping factor, the R versus l/A curves are shifted downwards toward lower resistances. From the slope of these linearly fitted R versus l/A curves, the resistivity, $\rho_{3d}=RA/l$, was extracted. The corresponding values are plotted in Fig. 6(a).

In addition to the four-terminal measurements, we also determined the nanowire resistance in a two-terminal configuration, particularly in cases where only two contact fingers could be placed on the nanowires. The corresponding values of ρ_{3d} determined from the slope of the linear R versus l/A fits are also included in Fig. 6(a). In general, ρ_{3d}, determined by both methods, systematically decreases with increasing doping factor. We attribute the deviations of ρ_{3d} occurring at some doping factors to the fact that for the four- and two-terminal measurements, different numbers of nanowires were measured. According to Fig. 6(b), a linear increase is observed above a doping factor of 50, if the conductivity σ_{3d} is plotted as a function of the doping factor.

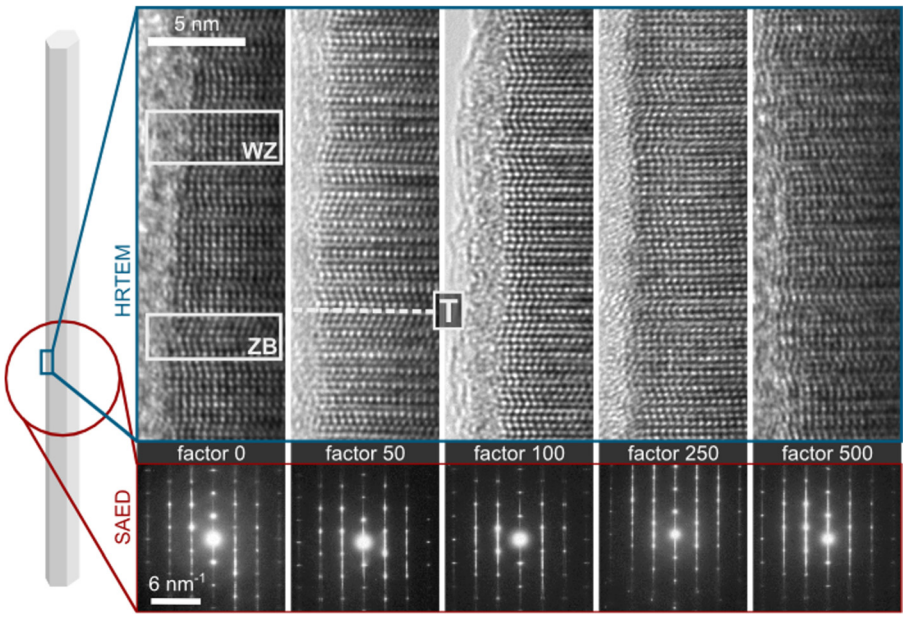

FIG. 4. (Color online) High resolution transmission electron micrographs (HRTEM) and selected area electron diffraction (SAED) patterns of InAs nanowires with doping factors of 0, 50, 100, 250, and 500. The sketch on the left side illustrates the relevant areas for TEM and SAED. Segments of wurtzite (WZ) and zinc blende (ZB) are exemplarily annotated in the left HRTEM image (doping factor 0). The line (T) in the following image marks a twinning boundary.

From the unintentionally doped nanowires to the ones with a doping factor of 500, the conductivity increased by a factor of about 25. At doping factors lower than 100 the conductivity levels off, possibly because of intrinsic bulk conductivity or because of the presence of a surface accumulation layer, due to Fermi level pinning within the conduction band.

In the inset of Fig. 6(a) the distribution of the normalized ρ_{3d} values for the wires with doping factors 1 and 250 are shown. Here, ρ_{3d} was determined for each individual wire measured in a four-terminal configuration. We find that with an increasing doping level the relative width of the distribution decreases. Since the measurements were performed in a four-terminal configuration, contributions of a varying contact resistance can be ruled out. A possible reason for the observed broad distribution might be found in the crystal structure. As can be seen in the transmission electron micrographs shown in Fig. 4, many stacking faults are present in the nanowire, which induce potential fluctuations in the conduction band along the wire axis. Most likely, each nanowire has an individual sequence of stacking faults and thus an

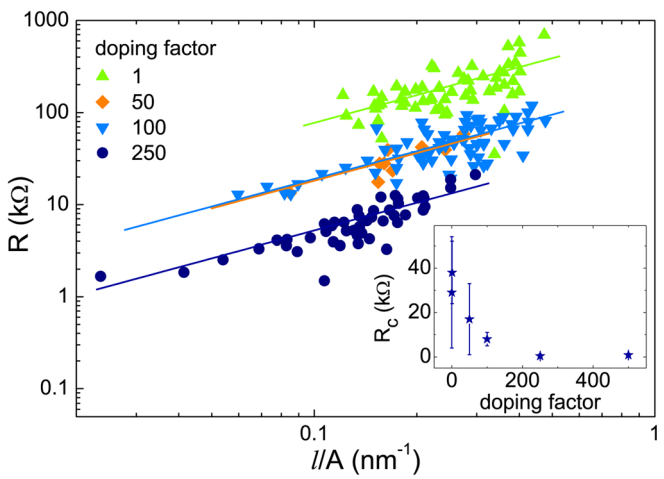

FIG. 5. (Color online) Room temperature four-terminal resistance, R, as a function of the distance of voltage probes to the cross section ratio, l/A, for wires with a doping factor of 1, 50, 100, and 250. The lines correspond to the linear fits for each doping factor. The inset shows the contact resistance, R_c, as a function of the doping factor.

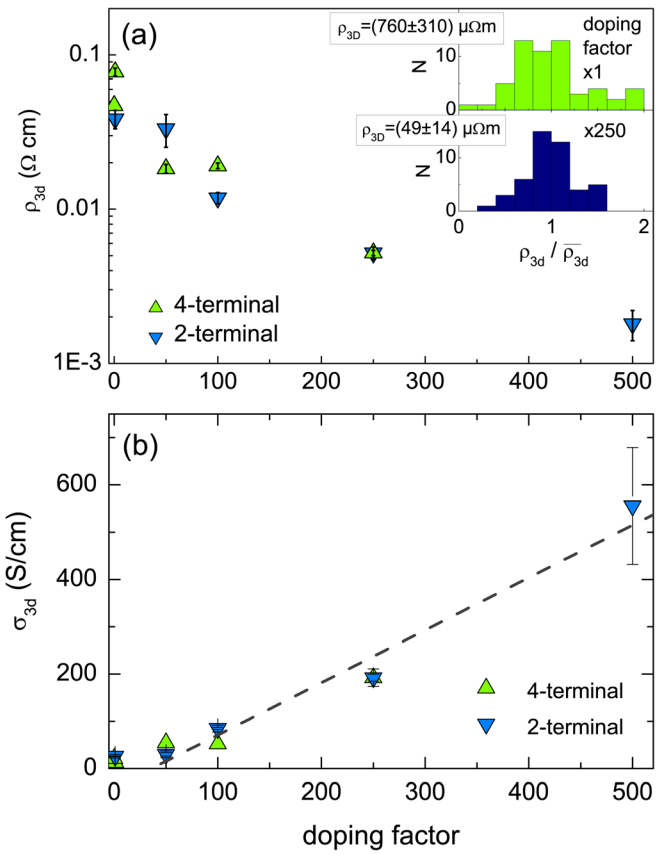

FIG. 6. (Color online) (a) Resistivity, ρ_{3d}, as a function of the doping factor extracted from measurements in two- and four-terminal configurations. The insets show the distribution of ρ_{3d} measured for the doping factors 1 and 250. (b) Corresponding conductivity, σ_{3d}.

individual potential profile. Thus, the number of carriers localized in the potential minima may vary from wire to wire, having the strongest impact on the conductivity for wires with lower carrier densities.

Two-terminal resistance measurements were used to obtain information on the total contact resistance, R_c, by extrapolating the resistance versus l/A toward zero contact separation. The respective values of R_c for different doping factors are given in Fig. 5 (inset). For doping factors 0 and 1 the contact resistance is found to be around 30 kΩ, with a relatively large spread of values. With an increasing doping factor, R_c systematically decreases until a value of 800 Ω is reached at the doping factor of 500. We attribute the lower contact resistance at larger doping factors to an increase of the Fermi energy in the nanowire and consequently a better coupling to the metallic contact.

In order to calculate the electron concentration, n_{3d}, in our nanowires, back-gate field-effect transistor measurements were performed. In Fig. 7 (left inset), typical drain current versus gate voltage (I_D-V_G) characteristics of nanowires with a doping factor of 1, 100, and 250 are shown. The threshold voltage, V_{th}, is determined by linear extrapolation. From the slope, μ_{FE} is determined.

The drain current, I_D, decreases along with the gate voltage, which confirms the *n*-type conductance. An *n*-type conductance was observed for the nanowires of all doping factors. At large negative gate voltages no complete pinch-off of the drain current was achieved, possibly caused by a by-pass channel due to an accumulation layer at the nanowire surface.[31] The electron concentration in the nanowire can be estimated from the threshold voltage, V_{th}, i.e., the gate voltage where the drain current is pinched off. Since in our case no complete suppression of I_D was achieved, V_{th} was extracted by extrapolation [cf., Figure 7, (left inset)]. The relation between n_{3d} and V_{th} is given by the following expression:

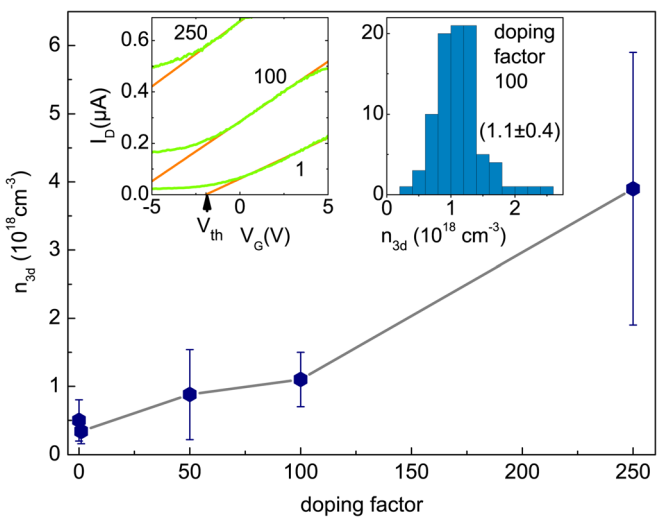

FIG. 7. (Color online) Electron concentration, n_{3d}, as a function of the doping factor. The left inset shows a transfer characteristic, I_D-V_G, for a nanowire with a doping factor of 1, 100, and 250. The threshold voltage, V_{th}, is found to be at about −1.9 V. The right inset presents the distribution of n_{3d} for a doping factor of 100.

$$n_{3d} = \frac{C|V_{th}|}{el\pi(d/2)^2} \quad (1)$$

The capacitance, C, between the nanowire and back-gate electrode is given by,[6,38]

$$C = \frac{2\pi\varepsilon_0\varepsilon l}{\ln[(2h+d+2\sqrt{h^2+hd})/d]} \quad (2)$$

with h the gate oxide thickness and $\epsilon = 3.9$ the dielectric constant of the SiO_2 layer. As can be seen in Fig. 7, the measured electron concentration increases monotonously from the mid-10^{17} cm^{-3} range for undoped nanowires to 3.9×10^{18} cm^{-3}. The data points plotted here follow a linear increase. Between the doping factors 50 and 250, an increase by a factor of 4.4 is found. For the doping factor of 500 no reliable value of n_{3d} could be determined because of the limited gate voltage range. The large error in n_{3d} for the doping factor of 250 can also be attributed to the uncertainty in determining V_{th}. As an example, for the set of wires with the doping factor of 100, the distribution of n_{3d} is depicted in Fig. 7 (right inset), with $n_{3d} = (1.1 \pm 0.4) \times 10^{18}$ cm^{-3}. It is known that the value of the back-gate capacitance, C, is only an upper limit, since in Eq. (2) a complete coverage of the nanowire with the gate electrode is assumed, while in our case the nanowire only lies on top of the dielectric SiO_2 layer. Finite element calculations by Wunnicke[39] showed that the actual capacitance is about a factor of 1.7 smaller than the value obtained from Eq. (2). An additional error in the values of n_{3d} enters because of interface states in the gate layer stacks, which are simultaneously recharged with the wire under the gate.[35] Therefore, the absolute values of n_{3d} presented in Fig. 7 can be considered as an upper limit and are systematically lower to a certain extent. Nevertheless, the observed tendency of an increase in electron concentration due to Si doping is correct.

In order to get a clearer picture of how the electrons are distributed in the nanowire, the electronic states in the wire were calculated by using a Schrödinger-Poisson solver.[17] In Fig. 8 (left inset), the conduction band profile and the carrier density, n, in the radial direction is shown for an undoped ($N_D = 0$) InAs nanowire. For the surface Fermi level pinning a value of 160 meV was assumed.[40,41] Due to surface Fermi level pinning, the conduction band is bent downwards at the surface. This induces a surface accumulation layer, indicated by the maximum of n at about 10 nm beneath the surface. For the nominally undoped nanowire an averaged electron concentration of 3×10^{17} cm^{-3} was extracted, which is close to the values obtained from the field-effect transistor measurements for the doping factors of 0 and 1. Since the background doping level of our material is expected to be in the range of 10^{14} cm^{-3} and thus, three orders of magnitude lower than the measured doping concentration, it is likely that the conduction electrons originate from the surface states. In contrast, as can be seen in the right inset in Fig. 8, for an assumed dopant concentration of $N_D = 1 \times 10^{18}$ cm^{-3} the electrons are almost uniformly distributed within the nanowire. Here, the average electron concentration, n_{3d}, of 9.7×10^{17} cm^{-3} was calculated, which is close to the values experimentally obtained for the doping factors of 50 and 100

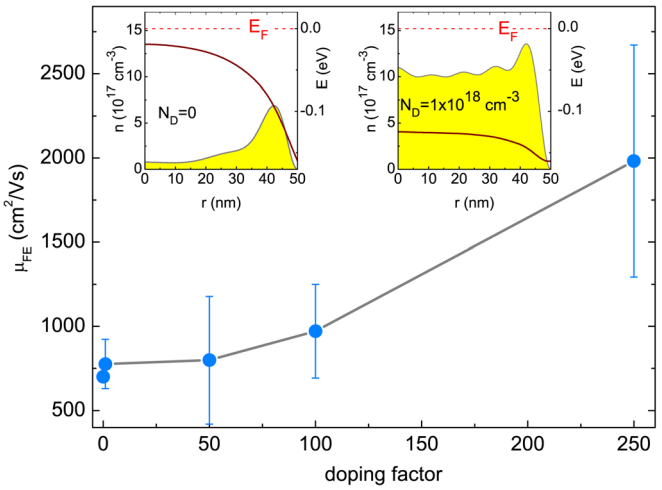

FIG. 8. (Color online) Field effect mobility, μ_{FE}, as a function of doping factor. The left and right inset shows the calculated electron density, $n(r)$, and the conduction band profile for an n-type doping of $N_D = 0$ and $N_D = 1 \times 10^{18}$ cm^{-3}, respectively. $r = 0$ corresponds to the wire center.

(cf., Figure 7). The comparison between the experimentally and theoretically determined values should be made with some caution, since the electronic states are probably also affected by the change of the crystal structure and corresponding polarization charges.[25]

In Fig. 8 the field effect mobility, μ_{FE}, is shown as a function of the doping factor. The mobility values are determined by using the following expression:

$$\mu_{FE} = g_m \frac{l^2}{C} \frac{1}{V_{SD}}, \tag{3}$$

with $g_m = \Delta I_D / \Delta V_G$ the maximum transconductance and V_{SD} the source-drain voltage. As one can infer from Fig. 7 (left inset), the maximum transconductance increases with the increasing doping factor. Thus, with the increasing doping concentration, μ_{FE} is found to increase from 780 cm^2/Vs at a doping factor of 1 to almost 2000 cm^2/Vs at a doping factor of 250.

The mobilities extracted here are comparable to or somewhat smaller than the values reported by other groups for InAs nanowires,[22,42,43] but considerably smaller than the values measured in epitaxial InAs layers.[44,45] One possible reason for the relatively low mobility compared to InAs layers might be the large density of stacking faults in our nanowires. Recently, Schroer and Petta[46] reported that with an increasing number of stacking faults, the mobility degrades. The additional scattering is caused by potential fluctuations, owing to the conduction band offset between wurtzite and zinc blende InAs[47–50] and also by polarization charges at the wurtzite/zinc blende interface.[25]

We attribute the increase of the field-effect mobility with the increasing doping factor to the change of carrier distribution within the nanowire. It was found by Affentauschegg and Wieder[41] that, due to the additional contribution of surface scattering, the mobility of electrons at the surface is considerably lower than the respective bulk value. As shown in Fig. 8 (left inset), for undoped nanowires the simulations yield a downward-bent conduction band with an accumulation layer at the surface. Since the electrons are primarily located close to the surface, surface scattering should play a major role. In contrast, for an assumed dopant concentration of $N_D = 1 \times 10^{18}$ cm^{-3} the electrons are almost uniformly distributed within the nanowire [cf., Figure 8, (right inset)]. Since in this case most carriers are located in the bulk of the nanowire, the detrimental effect of the surface scattering is reduced so that on average, the mobility is higher.[41] In addition to the effect described in the previous text, the improved screening of the potential fluctuations with increasing carrier density might also contribute to the increased mobility. Apparently, both contributions overcompensate for the additional electron scattering due to the increased number of ionized donors at larger doping concentrations.

B. Low temperature transport

As the temperature is lowered from room temperature to 4 K, the nanowire resistance of the moderately doped nanowires with a doping factor between 1 and 100 increases. This conclusion can be drawn from the dependence of the drain current on the source-drain voltage (I_D-V_{SD}), which is shown exemplarily in Figs. 9(a) and 9(b) for nanowires with a doping factor of 1 and 100, respectively. Obviously, the slope of the I_D-V_{SD} characteristics and thus the conductance decreases with decreasing temperature. Up to about 100 K, we find linear characteristics, while for lower temperatures a smaller slope around zero bias voltage is observed. Since the measurements were performed in a four-terminal configuration, an effect of the contacts on the characteristics can be excluded. We rather attribute the non-linear behavior to the onset of single electron tunneling.[11,46,51]

The temperature dependence of the resistivity ρ_{3d}, which was extracted from the slope of the I_D-V_{SD} characteristics, is plotted in Fig. 10(a). For moderate doping factors, i.e., 1 and 100, ρ_{3d} increases with decreasing temperature by a factor of 7.7 and 2.6, respectively, which is indicative of a semiconductor behavior. For the wire with a doping factor of 250, the resistivity increases by only 2%. In contrast, for the highest doping factor of 500, ρ_{3d} slightly decreases with decreasing temperature. Thus, with the increasing doping factor, a transition from a semiconductor-type to a metal-type temperature dependence is observed.

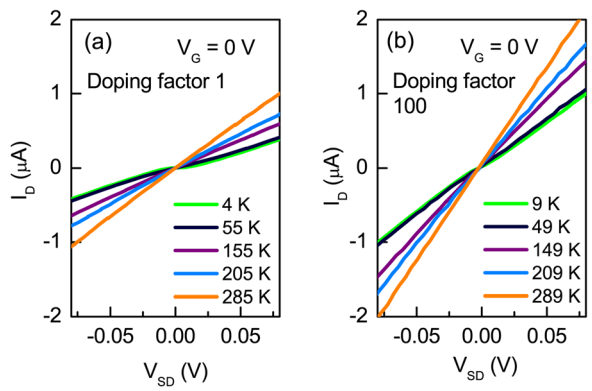

FIG. 9. (Color online) (a) Current-voltage characteristics of a nanowire with a doping factor of 1 at temperatures between 285 and 5 K. (b) Corresponding curve for a nanowire with a doping factor of 100.

In semiconductors a transition from semiconductor-type behavior to metal-type behavior occurs at the characteristic Mott electron concentration, n_c, which reflects the onset of electron wave function overlap.[52] The Mott transition occurs under the condition, $n_{3d}^{1/3} a_0 > 0.2$. Here, a_0 is the Bohr radius of a donor atom in InAs given by, $a_0 = 4\pi\hbar^2\varepsilon_0\varepsilon_r/m^* e^2$, with $\varepsilon_r = 15.15$ the dielectric constant InAs and $m^* = 0.023 m_e$ the effective electron mass. This yields $a_0 = 35$ nm. The transition is expected to occur at a concentration of only $n_c = 4 \times 10^{14}$ cm^{-3}, which is much lower than the electron concentrations determined, even for undoped nanowires. For $n_{3d} \geq n_c$, no thermal excitation is required to excite carriers into the conduction band. Consequently, in contrast to the observation a metal-type temperature dependence should be expected for all of our nanowires.

In order to further analyze the temperature dependence of the electron transport, the conductivity, σ_{3d}, is plotted in Fig. 10(b) as a function of the inverse temperature. As can be seen here, although the carrier concentration is substantially larger than n_c, a thermally activated enhanced conductivity, σ_{3d} is observed with decreasing $1/T$ for the nanowires with doping factors of 1, 100, and 250. At smaller inverse temperatures activation energies, E_a, of 12, 9.3, and 0.2 meV were extracted from a fit according to $\exp(-E_a/k_B T)$, respectively. Only for the nanowire with the doping factor of 500, a different temperature dependence of σ_{3d} was observed, i.e., a decrease of σ_{3d} with decreasing inverse temperature.

In principle, there are two possibilities which might explain the unexpected semiconductor-type behavior at low doping concentrations. As can be seen in the TEM images shown in Fig. 4, segments of different stacking order, i.e., zinc blende and wurtzite, are found in our nanowires. Band structure calculations for both crystal configurations demonstrated that the bandgap of the wurtzite-type InAs is slightly larger. This implies an offset in the conduction band at the boundary between the zinc blende and the wurtzite segments.[47,49,50] As illustrated in Fig. 10(a) (inset), the conduction band profile along the nanowire axis is expected to vary by the conduction band offset, ΔE_c. Regarding the value of ΔE_c, the calculations yield values between 23 meV (Ref. 50) and 86 meV.[47] These values are on the order of the excitation energies extracted from the temperature dependence of σ_{3d}. Depending on the electron concentration and thus, the position of E_F with respect to the conduction band edge, the carriers might have to overcome potential steps during transport along the wire. As can be seen in Fig. 8 (left inset), for undoped nanowires the Fermi level is a few meV above the conduction band in the center of the nanowire. Thus in this region, the transport might be thermally activated. However, due to a possible accumulation layer at the surface, a non-thermally activated by-pass channel might be present. For increasing electron concentrations, the Fermi energy increases so that the effective barrier height decreases. This is in accordance with the decrease of excitation energy for higher doping factors [cf., Figure 10(b)]. Since the total change of the conductance within the measured temperature interval is relatively weak, the presence of a parallel channel constituted by the surface accumulation layer is probable.

The second possibility for the thermally activated enhancement of the conductance is donor deactivation.[53] Here, the donor ionization energy increases with the decreasing nanowire radius when the Bohr radius is on the order of the nanowire radius. For our material system and nanowire dimensions we calculated the effect of donor deactivation following the theory of Diarra *et al.*[54] and found that it can be neglected in our case.

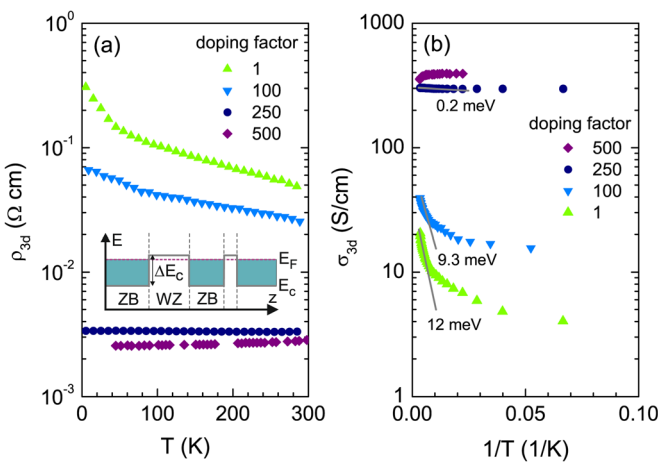

FIG. 10. (Color online) (a) Resistivity, ρ_{3d}, as a function of temperature for nanowires with doping factors of 1, 100, 250, and 500. (b) Corresponding plot of the conductivity, σ_{3d} vs inverse temperature. The inset in (a) illustrates the conduction band profile along the axis of the nanowire.

V. CONCLUSION

In summary, we successfully achieved *n*-type doping in selective area MOVPE grown InAs nanowires prepared in N_2 carrier gas. It is observed that doping systematically affects the nanowire morphology by reducing the nanowire length to the diameter (aspect) ratio. Even though doping does not systematically influence the wurtzite to zinc blende ratio in the wires—all wires still exhibit a high stacking fault density independent on the doping level—the conductivity and the carrier concentration could be monotonously increased. Doping was found to be very effective so that carrier concentrations in the 10^{18} cm^{-3} range could be achieved. Although even for the intrinsically doped nanowires and for wires with a moderate doping concentration the carrier concentration is beyond the Mott concentration, a thermally activated increase of the conductivity was observed. The underlying mechanism is not fully understood yet, however, there is a possible explanation in terms of potential fluctuations in the conduction band due to the change of the crystallographic stacking sequence from zinc blende to wurtzite. For the highest doping factor, a metal-type temperature dependence of the conductivity was found. Since well-controlled doping is one of the key ingredients of the electronic device design, our results can be regarded as an important step toward the realization of nanoelectronics based on semiconductor nanowires.

[1]J. Appenzeller, J. Knoch, M. T. Björk, H. Riel, H. Schmid, and W. Riess, IEEE Trans. Electron Devices **55**, 2827 (2008).
[2]C. Thelander, P. Agarwal, S. Brongersma, J. Eymery, L. F. Feiner, A. Forchel, M. Scheffler, W. Riess, B. J. Ohlsson, U. Gösele, and L. Samuelson, Mater. Today **9**, 28 (2006).
[3]W. Lu and C. M. Lieber, J. Phys. D: Appl. Phys. **39**, R387 (2006).

[4]K. Ikejiri, J. Noborisaka, S. Hara, J. Motohisa, and T. Fukui, J. Cryst. Growth **298**, 616 (2007).
[5]T. Bryllert, L.-E. Wernersson, T. Lowgren, and L. Samuelson, Nanotechnology **17**, 227 (2006).
[6]S. A. Dayeh, D. P. Aplin, X. Zhou, P. K. Yu, E. Yu, and D. Wang, Small **3**, 326 (2007).
[7]Q.-T. Do, K. Blekker, I. Regolin, W. Prost, and F. J. Tegude, IEEE Electron Device Lett. **28**, 682 (2007).
[8]C. Thelander, C. Rehnstedt, L. E. Froberg, E. Lind, T. Martensson, P. Caroff, T. Lowgren, B. J. Ohlsson, L. Samuelson, and L.-E. Wernersson, IEEE Trans. Electron Devices **55**, 3030 (2008).
[9]D. Candebat, Y. Zhao, C. Sandow, B. Koshel, C. Yang, and J. Appenzeller, 2009 67th Annual Device Research Conference (DRC), (The Pennsylvania State University, University Park, PA, 22–24 June 2009), pp. 13–14.
[10]T. Tanaka, K. Tomioka, S. Hara, J. Motohisa, E. Sano, and T. Fukui, Appl. Phys. Express **3**, 025003 (2010).
[11]S. D. Franceschi, J. A. van Dam, E. P. A. M. Bakkers, L. F. Feiner, L. Gurevich, and L. P. Kouwenhoven, Appl. Phys. Lett. **83**, 344 (2003).
[12]C. Fasth, A. Fuhrer, M. T. Björk, and L. Samuelson, Nano Lett. **5**, 1487 (2005).
[13]A. Pfund, I. Shorubalko, R. Leturcq, and K. Ensslin, Appl. Phys. Lett. **89**, 252106 (2006).
[14]J. A. van Dam, Y. V. Nazarov, E. P. A. M. Bakkers, S. D. Franceschi, and L. P. Kouwenhoven, Nature (London) **442**, 667 (2006).
[15]A. Fuhrer, C. Fasth, and L. Samuelson, Appl. Phys. Lett. **91**, 052109 (2007).
[16]T. Richter, Ch. Blömers, H. Lüth, R. Calarco, M. Indlekofer, M. Marso, and Th. Schäpers, Nano Lett. **8**, 2834 (2008).
[17]S. Estévez Hernández, M. Akabori, K. Sladek, Ch. Volk, S. Alagha, H. Hardtdegen, M. G. Pala, N. Demarina, D. Grützmacher, and Th. Schäpers, Phys. Rev. B **82**, 235303 (2010).
[18]S. Nadj-Perge, S. M. Frolov, E. P. A. M. Bakkers, and L. P. Kouwenhoven, Nature (London) **468**, 1084 (2010).
[19]H. Lüth, *Solid Surfaces, Interfaces and Thin Films* (Springer-Verlag, Berlin, Heidelberg, New York, 2010).
[20]R. Calarco and M. Marso, Appl. Phys. A **87**, 499 (2007).
[21]C. Blömers, Th. Schäpers, T. Richter, R. Calarco, H. Lüth, and M. Marso, Appl. Phys. Lett. **92**, 132101 (2008).
[22]A. C. Ford, J. C. Ho, Y.-L. Chueh, Y.-C. Tseng, Z. Fan, J. Guo, J. Bokor, and A. Javey, Nano Lett. **9**, 360 (2009).
[23]K. Sladek, A. Penz, K. Weis, S. Wirths, C. Volk, S. Alagha, M. Akabori, S. Lenk, M. Luysberg, H. Lüth, H. Hardtdegen, T. Schäpers, and D. Grützmacher, Mater. Res. Soc. Symp. Proc. **1258**, 2 (2010).
[24]K. A. Dick, P. Caroff, J. Bolinsson, M. E. Messing, J. Johansson, K. Deppert, L. R. Wallenberg, and L. Samuelson, Semicond. Sci. Technol. **25**, 024009 (2010).
[25]S. A. Dayeh, D. Susac, K. L. Kavanagh, E. T. Yu, and D. Wang, Adv. Funct. Mater. **19**, 2102 (2009).
[26]K. Tomioka, P. Mohan, J. Noborisaka, S. Hara, J. Motohisa, and T. Fukui, J. Cryst. Growth **298**, 644 (2007).
[27]K. Tomioka, J. Motohisa, S. Hara, and T. Fukui, Jpn. J. Appl. Phys. **46**, L1102 (2007).
[28]H. Paetzelt, V. Gottschalch, J. Bauer, G. Benndorf, and G. Wagner, J. Cryst. Growth **310**, 5093 (2008).
[29]M. Akabori, K. Sladek, H. Hardtdegen, Th. Schäpers, and D. Grützmacher, J. Cryst. Growth **311**, 3813 (2009).
[30]H.-Y. Li, O. Wunnicke, M. T. Borgström, W. G. G. Immink, M. H. M. van Weert, M. A. Verheijen, and E. P. A. M. Bakkers, Nano Lett. **7**, 1144 (2007).
[31]G. Astromskas, K. Storm, O. Karlström, P. Caroff, M. Borgström, and L.-E. Wernersson, J. Appl. Phys. **108**, 054306 (2010).
[32]C. Thelander, K. A. Dick, M. T. Borgström, L. E. Fröberg, P. Caroff, H. A. Nilsson, and L. Samuelson, Nanotechnology **21**, 205703 (2010).
[33]C. Gutsche, I. Regolin, K. Blekker, A. Lysov, W. Prost, and F. J. Tegude, J. Appl. Phys. **105**, 024305 (2009).
[34]J. Dufouleur, C. Colombo, T. Garma, B. Ketterer, E. Uccelli, M. Nicotra, and A. F. Morral, Nano Lett. **10**, 1734 (2010).
[35]T. Richter, H. Lüth, T. Schäpers, R. Meijers, K. Jeganathan, S. Estévez Hernández, R. Calarco, and M. Marso, Nanotechnology **20**, 405206 (2009).
[36]M. W. Larsson, J. B. Wagner, M. Wallin, P. H. Kansson, L. E. Fröberg, L. Samuelson, and L. R. Wallenberg, Nanotechnology **18**, 015504 (2007).
[37]R. de Picciotto, H. L. Stormer, L. N. Pfeiffer, K. W. Baldwin, and K. W. West, Nature (London) **411**, 51 (2001).
[38]J. Noborisaka, T. Sato, J. Motohisa, S. Hara, K. Tomioka, and T. Fukui, Jpn. J. Appl. Phys. **46**, 7562 (2007).
[39]O. Wunnicke, Appl. Phys. Lett. **89**, 083102 (2006).
[40]K. Smit, L. Koenders, and W. Mönch, J. Vac. Sci. Technol. B **7**, 888 (1989).
[41]C. Affentauschegg and H. H. Wieder, Semicond. Sci. Technol. **16**, 708 (2001).
[42]S. A. Dayeh, E. T. Yu, and D. Wang, Small **5**, 77 (2009).
[43]M. Scheffler, S. Nadj-Perge, L. P. Kouwenhoven, M. T. Borgström, and E. P. A. M. Bakkers, J. Appl. Phys. **106**, 124303 (2009).
[44]J. P. McCarthy, Solid-State Electron. **10**, 649 (1967).
[45]R. J. Harrison and P. A. Houston, J. Cryst. Growth **78**, 257 (1986).
[46]M. D. Schroer and J. R. Petta, Nano Lett. **10**, 1618 (2010).
[47]M. Murayama and T. Nakayama, Phys. Rev.B **49**, 4710 (1994).
[48]I. Vurgaftman, J. R. Meyer, and L. R. Ram-Mohan, J. Appl. Phys. **89**, 5815 (2001).
[49]Z. Zanolli, F. Fuchs, J. Furthmüller, U. von Barth, and F. Bechstedt, Phys. Rev. B **75**, 245121 (2007).
[50]A. De and C. E. Pryor, Phys. Rev. B **81**, 155210 (2010).
[51]A. A. Zhukov, Ch. Volk, A. Winden, H. Hardtdegen, and Th. Schäpers, JETP Lett. **93**, 13 (2011).
[52]N. Mott, Rev. Mod. Phys. **40**, 677 (1968).
[53]M. T. Björk, H. Schmid, J. Knoch, H. Riel, and W. Riess, Nature Nanotechnol. **4**, 103 (2009).
[54]M. Diarra, Y.-M. Niquet, C. Delerue, and G. Allan, Phys. Rev. B **75**, 045301 (2007).